Dielectric characterization of the water-matrix interaction in porous materials by thermal depolarization spectroscopy

Anthony N. Papathanassiou and John Grammatikakis
University of Athens, Department of Physics, Section of Solid State Physics, Papepistimiopolis, GR15784 Zografos, Athens, Greece
(Received 7 September 1999)

We investigate the dielectric behavior of sandstone, which consists of a porous matrix with a small amount of inherent humidity, by the thermal-stimulated depolarization current technique. Nine different relaxation mechanisms are detected by the thermal sampling scheme, and are characterized. The activation energy distribution and the pre-exponential factor are obtained by analyzing the signals under the constraint of a normal distribution in the activation energy. The drying of the specimen at elevated temperature under dynamic vacuum affects some of the relaxation mechanisms. The model of freely rotating dipoles may not account for all the drying-sensitive mechanisms. It is probable that water molecules are organized in a way that provide either conductive layers over the surface of the grains or for conductive inclusions inside the bulk. Long-distance charge-transport mechanisms are also affected by the removal of the humidity.

I. INTRODUCTION

During the last decade, there has been considerable interest in the dielectric properties of multiphase porous materials, which are either partially filled or saturated with fluids.[1–7] Sandstone has been employed widely as the porous matrix (host) material in such investigations.[1,3,5–7] It was observed that the dielectric behavior of the multicomponent rock-water system exhibits a polarization phenomenon which is probably due to the electrochemical interaction of the humidity with the grains' surface. A dispersion, which appears in the low-frequency region of the dielectric spectrum, is related to the humidity that coats the solid grains and provides diffusion paths.[4,6,8] The current assertion is that this low-frequency response is a ''bulk'' solid-liquid interfacial phenomenon, rather than an electrode effect.[1]

To the best of our knowledge, the vast majority of dielectric experiments has been performed in the frequency domain. In this sense, the formulation of the complex dielectric constant is employed: $\varepsilon^* = \varepsilon' - i\varepsilon''$, where ε^*, ε', and ε'' denote the complex dielectric constant, and its real and imaginary parts, respectively. Most researchers work with ε', so as to investigate the solid-liquid interaction phenomena.[1,3,4,6,7] On the other hand, the imaginary part ε'' of the dielectric constant, when plotted as a function of frequency, may reveal relaxation mechanisms. Unfortunately, despite the broad working frequency, the standard impedance spectroscopy is a low-resolution technique, and is unable to resolve the spectrum to its constituting individual relaxation mechanisms. Therefore it is hard to characterize the particular dispersions (i.e., to distinguish between dipole rotation, interfacial polarization, or long-distance charge transport) and evaluate the relaxation parameters of each response accurately.

In the present work, we employ the thermal-stimulated depolarization current (TSDC) scheme, which operates in the time domain and is equivalent to the low-frequency spectroscopy. TSDC spectroscopy is capable of detecting very weak responses and resolving different overlapping relaxations. It also has the unique advantage of selectivity: the choice of appropriate experimental conditions, in combination with the elimination of the undesirable contributions, may yield the detection of a particular single mechanism. Analyses of the TSDC signals lead directly to an evaluation of the relaxation parameters, which are the activation energy distribution and the pre-exponential factor.

In the present work, the elementary responses, which are responsible for the dielectric behavior of as-received sandstone, are identified. Characterization is attained by different TSDC modes. The removal of the inherent humidity from the pores' network affects the dielectric spectrum, and therefore, the relationship between the specific types of relaxation and different hydrophilic sites inside the porous material is revealed. The distribution in the values of the relaxation parameters is obtained experimentally through different experimental schemes and subsequent computer analyses. The activation energy is related to the height of the potential barrier that has to be overcome by the migrating free or bound charges, the broadening parameter σ represents the perturbation caused in the potential barriers, and the pre-exponential factor τ_0 yields the migration entropy.

II. THEORY

The dielectric relaxation of an insulator originates from the rotation of inherent permanent dipoles, the impedance of free-charge carriers from obstacles existing in the matrix (i.e., dislocations, grain boundaries, interfaces separating the conductive inclusions from the matrix) and the non-Ohmic sample-electrode interface, which leads to the space-charge formation.[9] The dielectric relaxation is characterized by the relaxation time τ. The temperature dependence of the relaxation time is usually described by an exponential Arrhenius law

$$\tau(T) = \tau_0 \exp\left(\frac{E}{kT}\right) \tag{1}$$

where E denotes the activation energy, τ_0 is the pre-exponential factor, and k is Boltzmann's constant.

In the TSDC method,[10] the depolarization current emitted by a previously polarized dielectric is recorded as a function of the increasing temperature of the sample. The *usual* mode is to polarize the specimen at a temperature T_p for a time interval $t_p \gg \tau(T_p)$. Subsequently, while keeping the external polarizing field on, the temperature is abruptly reduced to the liquid nitrogen temperature (LNT), where the relaxation time is practically infinite. As a result, upon removing the electric field, the dielectric remains polarized. Afterward, the sample is heated at a constant rate. The time (equivalently, temperature) variation of the polarization generates the depolarization current, which is recorded by a sensitive electrometer connected to the sample's surfaces. As soon as the thermal energy is enough to drive the polarized dipoles to a random orientation state, a transient electric signal is recorded, which is called a thermogram. Different types of dipoles (or the dispersion of the frozen space-charge polarization) produce additional peaks.

The depolarization current induced by the reorientation of noninteracting dipoles is:

$$I(T)=\frac{S\Pi_0}{\tau_0}\exp\left[-\frac{E}{kT}-\frac{1}{b\tau_0}\int_{T_0}^{T}\exp\left(-\frac{E}{kT}\right)dT\right], \quad (2)$$

where Π_0 is the initial polarization of the dielectric, S is the sample's surface area which is in contact with the electrode, T_0 coincides with the LNT, and b denotes the heating rate. The activation energy E is identical to the migration enthalpy h^m of the migrating bound charges.[11]

Transient electric signals are also obtained when the polarization mechanism is an interfacial or space-charge one.[12] The depolarization current originates from the annihilation of the polarization state (which was achieved when the sample was initially polarized), as temperature increases during the TSDC scan. It is assumed that the temperature dependence of the relaxation time τ on temperature is described by Eq. (1), but different curves (similar to the dipolar ones [see Eq. (2)] are obtained, depending on the model assumed to describe the polarization mechanism. The interfacial polarization is related to short-distance charge transport, and may be approximated by a long-dipole relaxation.

The description of the space-charge polarization is quite complicated. The free charge population undergoes different simultaneous processes, like space-charge-limited drift, diffusion, neutralization to the electrodes, creation and/or recombination of charges, etc.[12] It is also probable that the transferring charges are trapped by internal obstacles (traps) distributed in the bulk. The space-charge TSDC peaks are sensitive to the electrode material used, i.e., the blocking degree of the sample-electrode interface. The polarization state depends strongly upon the storage conditions and the electret's prehistory.[13] Although the competing mechanisms make it impossible to construct an analytical equation for the space charge TSDC signal, rough approaches have been made, and several approximate space-charge TSDC equations have been derived. The different approximations converge to the point that the initial edge of the space-charge TSDC curve coincides to that of the non-interacting rotating dipoles.[14]

The relaxation time τ can be evaluated from the relation (area method)

$$\tau(T)=\frac{1}{bI(T)}\int_{T}^{T_f}I(T)dT, \quad (3)$$

where T_f is the final temperature of the peak where the current becomes null. Equations (1) and (3) leads to the evaluation of the activation energy E and the factor τ_0, through a $\ln\tau(1/T)$ plot. For the initial part of the curve, Eq. (2) is well approximated by

$$I(T)\cong\frac{S\Pi_0}{\tau_0}\exp\left(-\frac{E}{kT}\right). \quad (4)$$

The initial rise of the $\ln I(1/T)$ data, when fitted to a straight line, yields the evaluation of E, via Eq. (4).

The contribution $\Delta\varepsilon$ of a specific relaxation mechanism to the dielectric constant of the material is

$$\Delta\varepsilon=\frac{Q}{\varepsilon_0 SE_p}, \quad (5)$$

where Q is the total charge released as the polarization annihilates, ε_0 is the permittivity of free space, and E_p is the intensity of the polarizing electric field. Q is identical to the area under the $I(t)$ peak, and is readily obtained through graphical integration of the thermogram.

If the activation energy is not single valued but has a Gaussian distribution around E_0, with distribution function[15,16]

$$f(E)=\frac{1}{\sqrt{2\pi}\sigma}\exp\left[-\frac{(E-E_0)^2}{2\sigma^2}\right], \quad (6)$$

where σ is the broadening parameter, the total depolarization current can be written

$$I(T)=\int_{-\infty}^{+\infty}f(E)I(T,E)dE, \quad (7)$$

where the term $I(T,E)$ is the monoenergetic TSDC equation [see Eq. (2)]. The integral of Eq. (2) can be approximated by the analytical expression

$$\int_{T_0}^{T}\exp\left(-\frac{E}{kT}\right)dT=\frac{T\exp(-E/kT)(E/kT+3.0396)}{(E/kT)^2+5.0364(E/kT)+4.1916}\Bigg|_{T_0}^{T}, \quad (8)$$

while the integration of Eq. (7) can be performed from 0 to $3E_0$.[15]

III. EXPERIMENTAL DETAILS

The experiments were performed in a vacuum cryostat, which operates from the LNT to 420 K. The specimens were placed inside the standard sample holder of the apparatus, that consists of two platinum electrodes. The depolarization current was measured by a Keithley 617 electrometer. The temperature was monitored via an Air Products temperature controller; a constant heating rate of 2 K/min was maintained during the heating stage. The electrometer and the temperature controller were connected to a computer.

Sandstone is a representative silicate porous material. The term ''as-received sample'' defines a specimen containing an inherent quantity of humidity, which is in equilibrium with

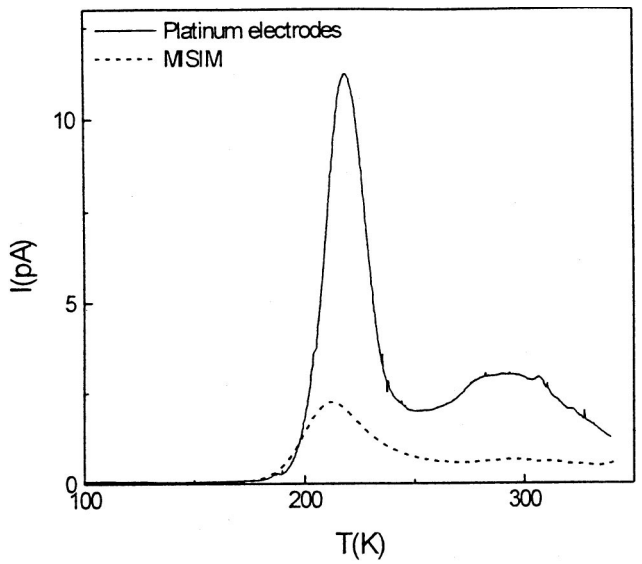

FIG. 1. Depolarization spectra of sandstone, when different type of electrodes are employed. The polarization conditions were $T_p = 296$ K, $E_p = 1$ kV/mm, and $t_p = 1$ min. MISIM electrodes are described in the text.

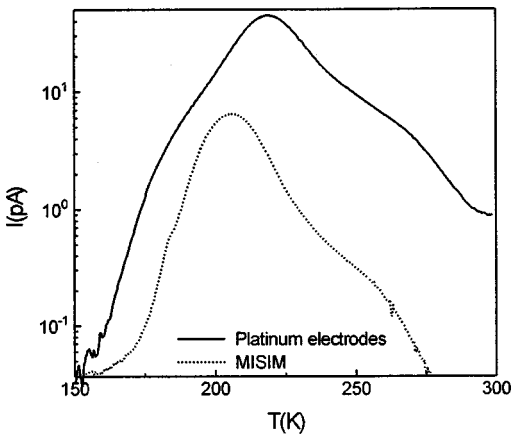

FIG. 2. Semilogarithmic plot of the signal obtained when the sample is polarized at $T_p = 240$ K, so as to eliminate the high-temperature contributions.

the normal air humidity. Such specimens have never been deliberately hydrated, i.e., by dilating the matrix through heating and inserting water under high pressure. The water content is definitely known through the reduction of the mass of the sample after drying. The composition of the sandstone is: 40-wt % quartz, 10-wt % amphibolite and pyroxene, 7-wt % glimmer mica, 16-wt % feldspars, and 27-wt % calcite. The porosity, obtained by optical microscopy on thin sections, was about 0.11. Typical dimensions of the specimens were 1 $cm^2 \times 1$ mm.

IV. RESULTS AND DISCUSSION

A couple of typical TSDC scans are presented in Fig. 1. Our investigation starts with the intermediate- and high-temperature regions, where strong dispersions appear that contribute considerably to the dielectric constant of the material. The study of the weak low temperature mechanisms follows in Sec. IV B.

A. Dominant relaxation mechanisms

The thermogram depicted in Fig. 1 is dominated by two broad and intense peaks, which are located at 219 K and close to room temperature, when platinum electrodes are employed. A somewhat similar signal appears when insulating (teflon) electrodes are used. We observe that the low-temperature peak shifts 7 K toward lower temperatures, and its amplitude is reduced to about 20% of the initial one. The dependence on the type of electrodes indicates that there exist space-charge contributions: the increase of the blocking degree of the electrodes, when placing teflon spacers between the sample's surfaces, and the metal electrodes of the apparatus [metal-insulator-sample-insulator-metal (MISIM) structure[17]] affects the discharge of the free-moving charges. At the same time, the accumulation of charge near the sample surfaces reduces the electric-field intensity inside the sample. The intensity of the high-temperature peak is reduced drastically and becomes a flat plateau (Fig. 1). Therefore, the latter peak is most probably related to the transport of charge through the thickness of the sample.

In order to hinder the high-temperature contributions, which likely originate from the space charge relaxation, we polarized the specimen at $T_p = 240$ K. By polarizing at sufficiently low temperature, the relaxation time of the high-temperature mechanisms becomes so long that the corresponding polarization state is negligible. In Fig. 2, we show two thermograms, each one corresponding to a different electrode material. The high-temperature peak becomes notably supressed. The semilogarithmic representation is indicative of different overlapping mechanisms. The appearance of the ''knees'' in the thermogram gives evidence of the presence of neighboring overlapping mechanisms. The reproducibility of the signal is moderate.

Thermal sampling. The broad relaxation spectrum was decomposed into its constituents by experimentally taking advantage of the ''selectivity'' the TSDC technique provides; different polarization and depolarization combinations may be employed to detect the desired elementary responses among many overlapping dispersions. The procedure is described in the literature as the ''thermal sampling technique.'' [17–19]

In the present work, we adopt an alternative thermal sampling technique:[20,21] At the temperature T_p, which is selected within the temperature range where a broad peak appears, the sample is polarized for the time interval t_p. Subsequently, the electric field is removed and the specimen is cooled immediately to the LNT. By polarizing at T_p, the slow relaxation mechanisms, which active at much higher temperatures than T_p, remain practically unpolarized. The subsequent discharge during the cooling results in the depolarization of the fast relaxation mechanisms, which activate at temperatures much lower than T_p. Consequently, only the mechanisms activating in the immediate neighborhood of T_p can reach a detectable polarization state. In the subsequent heating stage, a band, which corresponds to the polarized mechanisms that survived the polarization procedure and represents a portion of the initial dispersion, is recorded. The thermal sampling scheme is repeated for various T_p temperatures and a set of discrete responses is obtained.

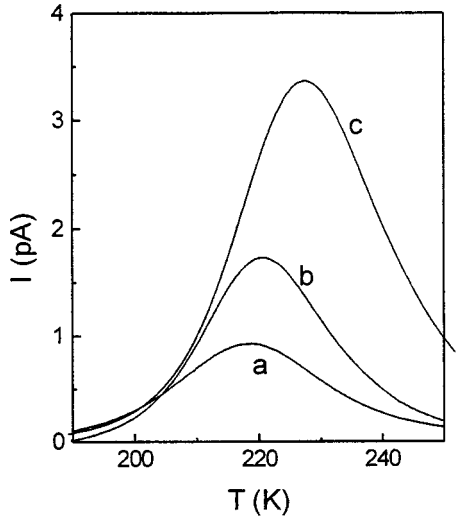

FIG. 3. A sample of thermal sampling responses, for different polarization temperatures $T_p = 205$ K (a), 210 K (b), and 220 K (c). The electric-field intensity was $E_p = 1$ kV/mm and the polarization time $t_p = 15$ s.

The interpretation of the thermal sampling experiments requires the construction of the $T_{\max}(T_p)$ diagram. Provided the TSDC peak is a single one [single relaxation time model; see Eq. (2)], then the maximum $T_{\max}$ of the responses would be independent of the polarization temperature T_p. If the TSDC signal is the overlap of two single relaxation mechanisms (without distribution in their relaxation parameters), the $T_{\max}$ points would accumulate around two distinct values. A random scatter of the experimental points is typical of space-charge mechanisms. The reproducibility of the thermal sampling peaks is representative of rotating dipoles. Conversely, space-charge components suffer from low reproducibility.

Some of the thermal sampling peaks are depicted in Fig. 3. In Fig. 4, the temperature $T_{\max}$, where the peak's maximum appears, versus the T_p temperature is shown. The maxima $T_{\max}$ distribute within certain intervals: 199–203, 214–220, 226–227, 241–242, and 259.5–298 K. The result is indicative of five relaxation mechanisms, labeled V, VI, VII, VIII, and IX, respectively (see Table I). We note that the above labeling is deliberately selected, in order to have a unified notation with the low-temperature mechanisms, which will be presented in Sec. IV B. The peaks corresponding to the VII mechanism reach a maximum at a temperature which is rather independent of the polarization temperature T_p. The same is valid for the VIII mechanism.

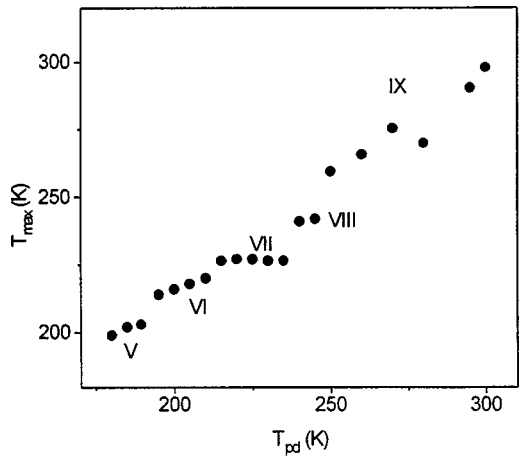

FIG. 4. The temperature $T_{\max}$ where the current reaches a maximum, as a function of the polarization temperature T_p. The signals were obtained by the thermal sampling scheme.

TABLE I. Components of the strong dispersions recorded in the intermediate- and high-temperature regions of the TSDC spectrum. The signals were obtained by applying the thermal sampling scheme, as mentioned in the text. The data were analyzed assuming that the activation energy obeys a Gaussian distribution around a central value E_0, with a broadening parameter σ.

	T_p (K)	$T_{\max}$ (K)	E_0 (eV)	σ (eV)	τ_0 (s)
V	180	199	0.571	0.021	6.84×10^{-13}
	185	202	0.592	0.018	3.42×10^{-13}
	189.5	203	0.579	0.001	7.17×10^{-13}
VI	195	214	0.590	0.019	2.45×10^{-12}
	200	216	0.591	0.019	3.10×10^{-12}
	205	218	0.610	0.023	1.65×10^{-12}
	210	220	0.590	0.018	7.10×10^{-12}
VII	215	226.5	0.603	0.028	1.23×10^{-11}
	220	227	0.611	0.021	7.30×10^{-12}
	225	227	0.612	0.020	5.47×10^{-12}
	230	226.5	0.619	0.019	2.79×10^{-12}
	235	226.5	0.610	0.021	4.09×10^{-12}
VIII	240	241	0.743	0.038	8.17×10^{-14}
	245	242	0.742	0.038	1.60×10^{-13}
IX	250	259.5	0.781	0.044	2.25×10^{-13}
	260	265.8	0.790	0.045	2.83×10^{-13}
	270	275.5	0.792	0.032	9.71×10^{-13}
	280	270	0.784	0.038	8.47×10^{-13}
	295	290.5	0.813	0.042	2.72×10^{-12}
	300	298	0.815	0.041	4.80×10^{-12}

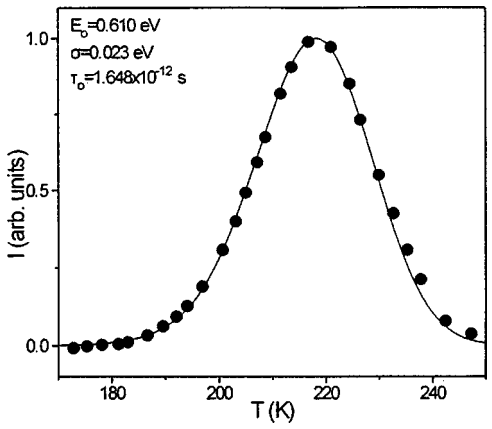

FIG. 5. The theoretical curve that best matches the (normalized) data points, obtained by the thermal sampling. The theoretical model assumes that the activation energy is not single valued, but is distributed around a central value E_0. The experimental thermal sampling response was obtained by polarizing at $T_P = 205$ K for the time interval $t_P = 15$ s. The specimen was subsequently cooled to the LNT in the absence of an electric field.

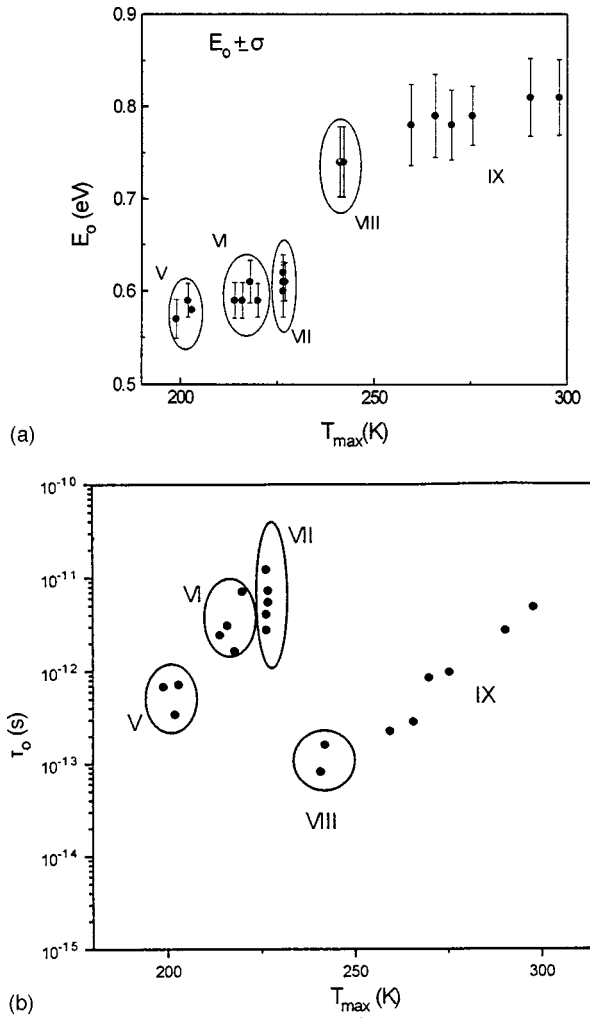

FIG. 6. (a) Temperature distribution of the activation energy E_0, obtained by full-curve fitting on the thermal sampling signals. The vertical bars represent the broadening parameter σ. (b) Temperature distribution of the pre-exponential factor τ_0, obtained by full-curve fitting on the thermal sampling signals.

Evaluation of the relaxation parameters. Each thermal sampling response was analyzed assuming that the activation energy value is not single valued but follows a normal distribution around a central value E_0. We employed a nonlinear least-squares fit program so as to obtain a theoretical curve that best matches the experimental data. The result was visually inspected to ensure a fine match of the initial rise part of the theoretical curve to the experimental points, since the low-temperature region is less sensitive to the distribution function selected than the sensitive end tail of the thermogram. In Fig. 5, we show a representative signal obtained by the thermal sampling technique, together with a theoretical curve that best matches the experimental data points. The central values of the activation energy E_0, which are obtained by the full curve fitting, are displayed in Fig. 6(a) in relation to the temperature $T_{\max}$, where each signal exhibits a maximum. The broadening parameters σ are represented by vertical bars of length 2σ. We note that the activation energy values accumulate around five distinct regions, which correspond to the five relaxation mechanisms initially identified via the $T_{\max}(T_p)$ diagram (Fig. 4). In Fig. 6(b) we have plotted the pre-exponential factor τ_0 vs the temperature $T_{\max}$. Table I lists the set of E_0, σ, and τ_0 for each relaxation mechanism.

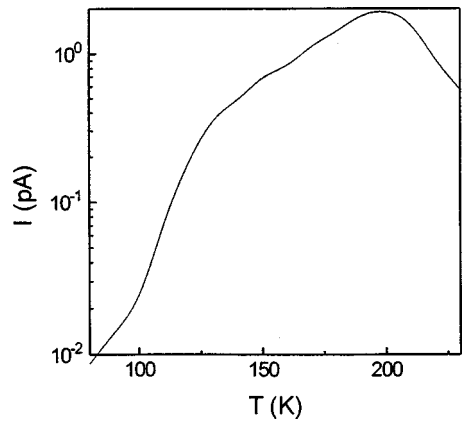

FIG. 7. Semilogarithmic plot of the spectrum obtained when the polarization temperature is $T_P = 200$ K. The ''knees'' indicate the presence of overlapping peaks.

B. Low-temperature region

The low-temperature spectrum, which is obtained by polarizing at $T_p = 200$ K, is depicted in Fig. 7. The depolarization current is considerably lower than that recorded in the intermediate and high-temperature regions. The ''knees'' in the semilogarithmic plot indicate the presence of multiple overlapping mechanisms. The temperature region below 200 K is usually labeled as the low-temperature LT territory of the dielectric relaxation spectrum. In a series of paper[22–27] we showed that the polarization within the LT region can hardly activate the undesirable high-temperature space-charge contributions. The LT mechanisms are most probably due to dipole relaxation.

At the temperature $T_p = 150$ K, we polarized with an electric field of intensity $E_p = 2.5$ kV/mm for the time interval $t_p \approx 1$ s, and cooled to the LNT. The thermogram obtained is depicted in Fig. 8(a). The signal consists of two overlapping mechanisms, labeled I and II, respectively, in accordance with the notation employed for the labeling of the intermediate and high temperature region. Dispersion I was traced by simply polarizing at $T_p = 125$ K. We repeated the experiment under the aforementioned polarization conditions, but, in the heating stage, we discharged up to 150 K and immediately afterwards, we cooled once more to the LNT. A final run revealed a clear single maximum located at 155 K (mechanism II). In Figs. 8(b) and 8(c) we show the signals corresponding to the I and II mechanisms, respectively, together with the theoretical curves that best fits the experimental data points. The relaxation parameters are listed in Table II.

In Fig. 9, another relaxation mechanism (dispersion III), that exhibits a maximum at 174.5 K, is displayed. The polarization state was achieved by polarizing at $T_p = 160$ K for the time interval $t_p = 1$ min. An efficient cleaning from the lower-temperature mechanisms was achieved by discharging from the LNT up to 165 K. Figure 9 also shows the theoretical curve that best matches the experimental data points, and the relaxation parameters are included in Table II.

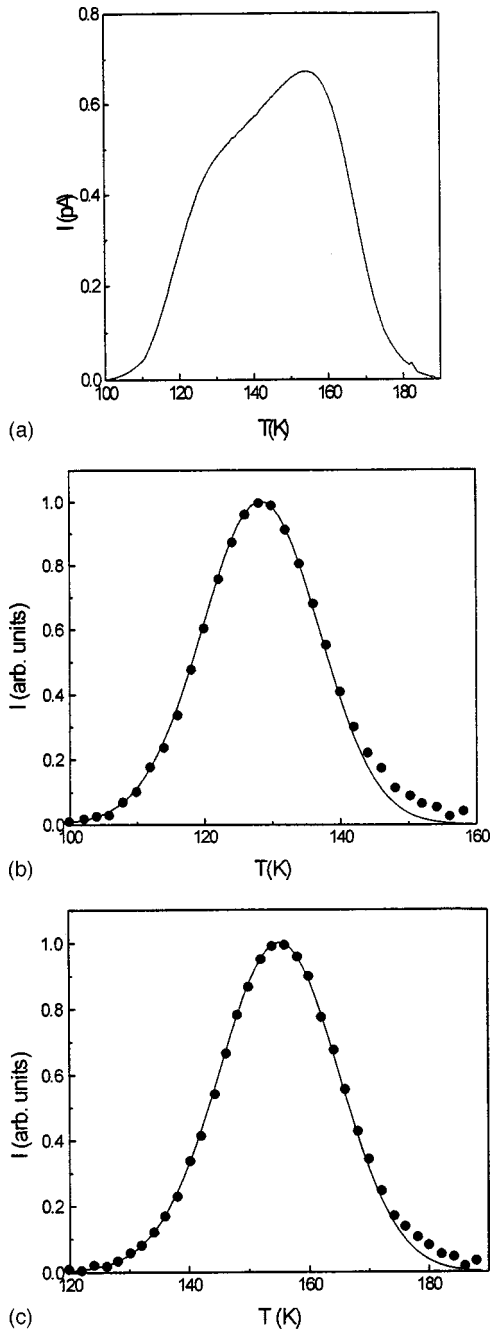

FIG. 8. (a) The signal obtained by polarizing at $T_p = 150$ K, with an electric field of intensity $E_p = 2.5$ kV/mm for the time interval $t_p \approx 1$ s. (b) Theoretical curve fitted to the data points corresponding to relaxation I, which was obtained by selective polarization. (c) Theoretical curve fitted to the data points (II relaxation) obtained by selective polarization and partial discharge of the undesirable low-temperature dispersion.

By polarizing at $T_p = 180$ K for the time interval $t_p \approx 1$ s, and discharging from the LNT to 180 K, the mechanism depicted in Fig. 10 was isolated. In Table II, we show the relaxation parameters obtained from the analysis of the signal. It was hard to fit a theoretical curve to the entire set of the data points. The low-temperature part of the signal is less sensitive to the undesirable high-temperature contribution, so we emphasized an adequate visual match of the theoretical curve to the data points which are located below the maximum temperature T_{max} (Fig. 10).

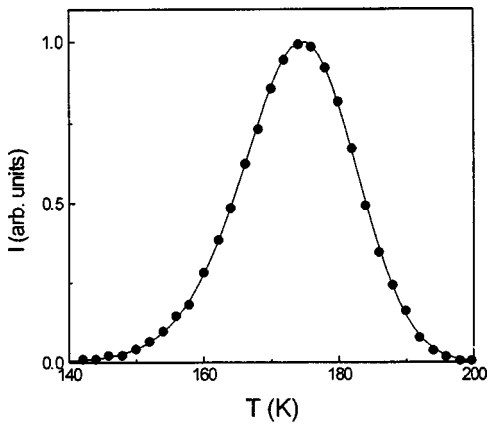

FIG. 9. The III relaxation mechanism (data points). The polarization conditions were $T_p = 160$ K, $E_p = 1$ kV/mm, and $t_p = 1$ min. The low-temperature neighboring relaxations were discharged from the LNT to 165 K. The solid line is the theoretical curve that best matches the experimental points.

C. Effect of drying

The samples were placed inside a vacuum chamber and were dried at 373 K for 24 h. The vacuum, which was maintained by a turbomolecular vacuum pump, was about 10^{-7} bar. The loss of weight of the specimens was 0.26%. In Fig. 11, we display the thermogram obtained from an as-received specimen, together with that recorded immediately after the drying procedure. It is obvious that the signal is significantly suppressed after drying the specimen.

In Table III, we display the percentage reduction of the amplitude of each individual relaxation mechanism. The charge released throughout the TSDC scan is given by the integral $\int_0^{t^*} I(t)dt$, where t^* is the time duration of the TSDC scan.

We found that the total charge released by the dried sample is 9% of that released by the as-received specimen. By using Eq. (5), we evaluated the contribution of the entire group of relaxation mechanisms detected by the TSDC spectroscopy, to the value of the dielectric constant: $\Delta\varepsilon = 38.6$ for the as-received sandstone and $\Delta\varepsilon = 3.5$ for the dry one.

Let us assume that the water molecules, which were extracted from the pore network, could rotate initially freely in

TABLE II. Information about the polarization and discharging of undesirable components that lead to peak cleaning in the low-temperature territory, together with the relaxation parameters. The data were analyzed assuming a normal distribution in the activation energy values.

	Peak cleaning scheme			Relaxation parameters			
	T_p (K)	t_p (s)	Discharge	T_{max} (K)	E_0 (eV)	σ(eV)	τ_0 (s)
I	125	≈ 1	none	128	0.320	0.018	2.41×10^{-11}
II	150	≈ 1	from LNT to 150 K	155	0.406	0.022	6.97×10^{-12}
III	160	60	from LNT to 165 K	174.5	0.446	0.015	1.97×10^{-11}
IV	180	≈ 1	from LNT to 180 K	188.5	0.535	0.009	7.08×10^{-13}

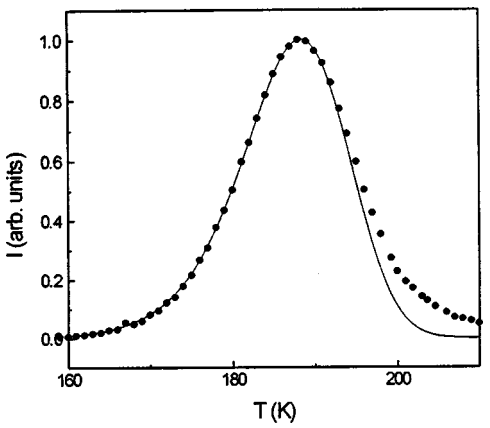

FIG. 10. By polarizing at $T_p = 180$ K for the time interval $t_p \approx 1$ s and discharging from the LNT to 180 K, we isolated the mechanism IV (data points). The solid line is the theoretical curve that best matches the experimental points.

the matrix. From the reduction of the charge released, we obtained an estimate of the mass of humidity, which is ten times smaller than the value calculated from the loss of mass that was measured by the gravitometric method. The latter estimation indicates that the model of freely rotating water dipoles can hardly account for the entire set of the relaxation mechanisms which are sensitive to the drying. It is probable that water molecules are organized in such way that conductive inclusions or conducting layers around the grains are formed inside the matrix. Then the polarization might be characterized as a Maxwell-Wagner one.

D. Attribution of the relaxation mechanisms

In reference to Table III, dispersion I is eliminated almost completely by drying whereas dispersion II reduces to 70% of its initial amplitude. The temperature region where the latter mechanisms activate is typical of relaxation of dipoles, which are either water molecules or composed of hydroxyl units.[25] The decrease of the polarizable entities on drying strengthens the latter assertion. Relaxation III is rather insensitive to the pore evacuation, and might be attributed to the rotation of permanent defect aggregates inside the matrix.

The height of peak IV decreases after the thermal anneal. However, we observed that relaxation IV is not modified when the specimen is outgassed at room temperature for a long period of time. Therefore, the modification of the band results from merely the thermal perturbation. On the other hand, comparative TSDC studies on calcite, dolomite, and magnesite have led to the conclusion that a peak located at 188 K, with energy parameters $E = 0.53$ eV and $\tau_0 = 1.22 \times 10^{-11}$ s,[23] is related to the rotation of point defect agglomerates, which are favored by the calcium carbonate sublattice.[22,23,25] The activation energy value is about 1% different from that reported in Table III for the IV relaxation. An order of magnitude difference in the pre-exponential factor is attributed to the error in determining its value, and to the perturbation caused in the calcium carbonate lattice by the mixing with the other constituents of sandstone. The dependence of the peak amplitude upon thermal perturbation is typical of point defect dipoles. Recalling that calcite contributes 27 wt.% to the composition of the sandstone, in combination with the above-mentioned observations about the peak position and its relaxation parameters, it is reasonable to state that peak IV is produced by the calcium carbonate component.

TABLE III. Percentage reduction of the peak amplitude, following the extraction of the humidity from the pore network.

	I	II	III	IV	V	VI	VII	VIII	IX
$\left\|\frac{\Delta I_{max}}{I_{max}}\right\|$%	100	30	2	16	99	96	82	70	50

The intense responses V, VI, and VII are dramatically suppressed after the drying procedure (Table III). We speculate that they are related to the humidity extracted from the pore network. Among the three aforementioned dispersions, relaxation VII has a maximum T_{max}, which is practically independent of the polarization temperature T_p. The analyses of the thermal sampling signals yield identical values of E_0 and τ_0, within the experimental errors. This situation is typical of mechanisms which are characterized by a single relaxation time value. Therefore, the values of the broadening parameters σ results from the undesirable neighboring relaxations and do not inherently characterize the dominant mechanism. The $T_{max}(T_p)$ diagram and the full curve-fitting analyses indicate that the relaxation process which is related to the VII hydrophilic dispersion is potentially different than those corresponding to the V and VI mechanisms. If the polarizable entities of VII mechanisms were freely rotating water dipoles, they would produce a TSDC signal within the low-temperature region, but this is not the case. Therefore, one should seek different types of interfacial polarization. Two different types of polarization may take place within the pore network:[1,3,4] one is related to the immediate distribution of humidity over the solid frame, and the other involves the subsequent hydration of the porosity. The first set of water molecules is expected to be more strongly bound to the matrix than the second one, and less easily removed from the

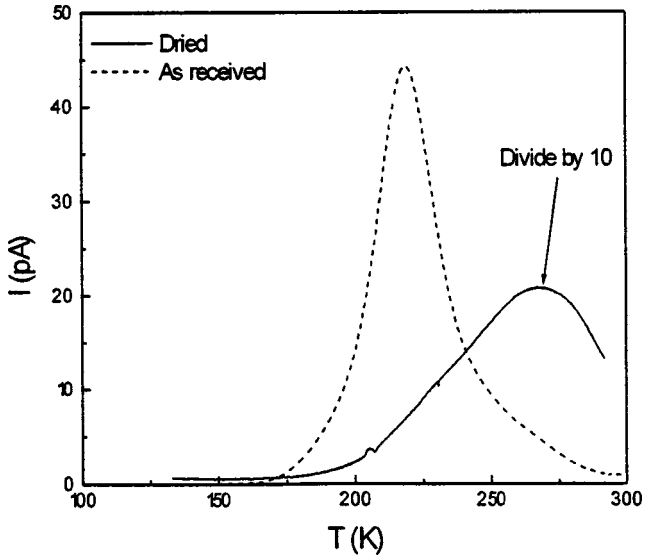

FIG. 11. The TSDC signal recorded in a dry sample of sandstone, together with the thermogram recorded from an as-received specimen.

porous material. Additionally, the relaxation time for the VII relaxation, which appears at higher temperature than the dispersions V and VI, is larger than that of the latter ones, assisting the hypothesis of a strongly bound layer attached directly to the surface of the grains. Hence dispersion VII might be related to a polarization operating in the humidity layer that is directly attached to the grains' surface, while V and VI are related to relaxation processes occurring in additional stratified humidity layers.

Dispersions VIII and IX are well understood from the preliminary TSDC experiments. They are both strongly sensitive to the nature of the electrodes used (Fig. 1). In particular, their amplitudes are drastically diminished when insulating (teflon) electrodes are employed. Additionally the signals are irreproducible, even if the polarization conditions are kept constant in different TSDC experiments. The behavior is typical for space charge mechanisms. Dispersions VIII and IX correspond to two different modes of long-distance charge transport. It is difficult to find a firm relation between the strength of the mechanisms and the role of humidity, because of the low reproducibility of the peaks. However, Table III indicates that both mechanisms are enhanced by the humidity. It is more obvious that dispersion VIII is strengthened by the presence of water molecules. The energy distribution is narrower than that exhibited by dispersion IX, and its relaxation time is lower than that of the higher-temperature one. It is probable that mechanism VIII is related to a fast grain boundary diffusion, whereas humidity provides additional charge carriers and additional migration paths for mechanism IX.

V. CONCLUSIONS

In the present work we experimentally investigated the relaxation in multicomponent porous sandstone with inherent humidity. We characterized the dielectric responses by certain experimental schemes and by estimating the profiles of the relaxation parameters, together with a thorough visualization of the physical aspects about the polarization phenomena. We found that humidity is responsible for the large value of the dielectric constant of as-received sandstone. The relative intensities of the low-temperature dipolar dispersions, in relation to the relaxations operating at intermediate temperatures, indicate that the organization of the water molecules is different than that of freely rotating dipoles, and that they are organized in a way that might be described by the interfacial polarization. We traced three different relaxations, which might be related to three different modes of the latter polarization. VII relaxation is characterized by large values of the relaxation time and is less suppressed after drying, in comparison to mechanisms V and VI. Hence we attribute the VII dispersion, which is relatively strongly bound to the grains' surface, to the polarization related with the direct solid-liquid interface. Mechanisms V and VI are related to secondary states of hydration. Two long-distance charge transport mechanisms (dispersions VIII and IX), which are enhanced by the presence of humidity, operate in the high-temperature region.

ACKNOWLEDGMENT

A.N.P. would like to thank the State Scholarship Foundation IKY, Greece, for financial support.

[1] B. Nettelblad and G. A. Niklasson, J. Phys.: Condens. Matter **8**, 7049 (1996).
[2] B. Nettelblad, J. Appl. Phys. **79**, 7106 (1996).
[3] B. Nettelblad and G. A. Niklasson, J. Phys.: Condens. Matter **7**, L619 (1995).
[4] R. Knight and A. Abad, Geophysics **60**, 431 (1995).
[5] A. L. Endres and R. Knight, J. Appl. Phys. **69**, 1091 (1991).
[6] R. Knight and A. Endres, Geophysics **55**, 586 (1990).
[7] R. Knight and A. Nur, Geophysics **52**, 644 (1987).
[8] W. C. Chew and P. N. Sen, J. Chem. Phys. **77**, 4683 (1982).
[9] A. K. Jonscher, *Dielectric Relaxation in Solids* (Chelsea Dielectrics Press, London, 1983).
[10] C. Bucci and R. Fieschi, Phys. Rev. Lett. **12**, 16 (1964).
[11] P. A. Varotsos and K. D. Alexopoulos, in *Thermodynamics of Point Defects and Their Relation with Bulk Properties*, edited by S. Amelinckx, R. Gevers, and J. Nihoul (North-Holland, Amsterdam, 1985).
[12] J. Vanderschueren and J. Gasiot, in *Thermally Stimulated Relaxation in Solids*, edited by P. Braunlich (Springer-Verlag, Berlin, 1979).
[13] J. van Turnhout, *Thermally Stimulated Discharge of Polymer Electrets* (Elsevier, Amsterdam 1975).
[14] P. Müller, Phys. Status Solidi A **67**, 11 (1981).
[15] J. P. Calame, J. J. Fontanella, M. C. Wintersgill, and C. Andeen, J. Appl. Phys. **58**, 2811 (1985).
[16] E. Laredo, M. Puma, N. Suarez, and D. R. Figueroa, Phys. Rev. B **23**, 3009 (1981).
[17] J. van Turnhout, in *Electrets*, edited by G. M. Sessler (Springer-Verlag, Berlin, 1980).
[18] T. Nedetzka, M. Reichle, A. Mayer, and H. Vogel, J. Phys. Chem. **74**, 2652 (1970).
[19] M. Zielinski and X. Kryszewski, J. Electrost. **3**, 69 (1977).
[20] S. Schräder and H.-E. Carius, in *Proceedings of the 7th International Symposium in Electrets ISE7*, edited by R. Gerhard-Multhaupt, W. Kunstler, L. Brehmer, and R. Danz (Berlin, 1991), p. 581.
[21] A. N. Papathanassiou, J. Grammatikakis, and N. Bogris, Phys. Rev. B **48**, 17 715 (1993).
[22] A. N. Papathanassiou, J. Grammatikakis, V. Katsika, and A. B. Vassilikou-Dova, Radiat. Eff. Defects Solids **134**, 247 (1995).
[23] A. N. Papathanassiou and J. Grammatikakis, Phys. Rev. B **53**, 16 252 (1996).
[24] A. N. Papathanassiou and J. Grammatikakis, J. Phys. Chem. Solids **58**, 1063 (1997).
[25] A. N. Papathanassiou and J. Grammatikakis, Phys. Rev. B **56**, 8590 (1997).
[26] A. N. Papathanassiou, J. Phys. Chem. Solids **60**, 407 (1999).
[27] N. Bogris, J. Grammatikakis, and A. N. Papathanassiou, Phys. Rev. B **58**, 10 319 (1998).